

Rotational damping in a multi- j shell particles-rotor model

Lu Guo,^{1,*} Jie Meng,² En-Guang Zhao,³ and Fumihiko Sakata⁴

¹*Department of Mathematical Science,*

Ibaraki University, Mito 310-8512, Ibaraki, Japan

²*School of Physics, Peking University, Beijing 100871, China*

³*Institute of Theoretical Physics, Chinese Academy of Sciences, Beijing 100080, China*

⁴*Institute of Applied Beam Science,*

Graduate School of Science and Engineering,

Ibaraki University, Mito 310-8512, Ibaraki, Japan

(Dated: December 16, 2018)

Abstract

The damping of collective rotational motion is investigated by means of particles-rotor model in which the angular momentum coupling is treated exactly and the valence nucleons are in a multi- j shell mean-field. It is found that the onset energy of rotational damping is around 1.1 MeV above yrast line, and the number of states which form rotational band structure is thus limited. The number of calculated rotational bands around 30 at a given angular momentum agrees qualitatively with experimental data. The onset of rotational damping takes place gradually as a function of excitation energy. It is shown that the pairing correlation between valence nucleons has a significant effect on the appearance of rotational damping.

PACS numbers: 21.10.Re, 23.20.Lv, 27.70.+q

*Electronic address: guolu@mcs.ibaraki.ac.jp

I. INTRODUCTION

The experimentally observed rotational bands often lie in the region near yrast line and are described as particle-hole excitations in the mean-field. At higher excitation energy above the yrast line, it does not necessarily form rotational band structure due to the damping of collective rotational motion [1, 2]. When the rotational damping takes place, E2 transition from an excited state spreads out over many final states. The gamma-rays which are emitted from the above excited region can not be distinguished as discrete peaks, thus forming a quasi-continuum spectra. Experimentally rotational damping has been studied through the analysis of quasi-continuum spectra [3, 4, 5, 6, 7]. Recent experimental progress in high precision three-dimensional gamma-ray correlation measurements makes it possible to study various features of collective rotational motion in the regions of discrete rotational bands and damped rotational motion [8, 9, 10, 11, 12, 13, 14, 15]. In particular, the newly developed fluctuation analysis method [8, 9] has presented the number of rotational bands existing in a rare-earth nucleus is only about 30 at a given angular momentum, thus confirming the occurrence of rotation damping.

Early theoretical studies on rotational damping [1, 2, 16, 17] showed that with the increase of level density the off-diagonal residual interaction becomes effective to cause mixing of many-particle many-hole configurations in the rotating mean-field. Since different configurations respond differently to the Coriolis force, the configuration mixing results in a dispersion of rotational frequency within each energy eigenstate, implying a damping of the collective rotational motion. However, in these works [1, 2, 16, 17], the assumption that configuration mixing is described by the general statistical theory of random matrices has been used to treat the E2 strength function associated with the damped rotational motion.

Recent studies on the microscopic structure and mechanism of rotational damping have been done extensively for normally deformed and superdeformed nuclei in the cranked Nilsson mean-field combined two-body residual interaction [18, 19, 20, 21, 22, 23, 24, 25]. In these discussions, the excited rotational bands are described as intrinsic many-particle many-hole excitations in the cranking Nilsson mean-field. In order to obtain rotational damping, the bands are mixed by two-body residual interaction. Furthermore, the cranking model is semi-classical and the angular momentum is not a good quantum number.

One can also use the particles-rotor model (PRM) to obtain the band structure as well

as rotational damping and to study the coupling between single-particle degree of freedom and collective rotational motion. Moreover as noted in Ref. [19], PRM is more appropriate on angular momentum coupling in wave functions and E2 transition matrix elements, since angular momentum is not a conserved quantity in cranking model. With many particles in a single- j shell, a systematic comparison of cranking model and PRM has been done and the pair-correlation transition in rotating nuclei has been investigated in Ref. [26]. In Ref. [27], PRM has been used to examine the quality of the tilted axis cranking and its interpretation. In particular, by correctly treating the angular momentum coupling in triaxial PRM, a new phenomenon-chiral doublet bands has been predicted [28] and verified later by experiment. Therefore it will be interesting to study the rotational damping by PRM. The nuclear chaotic behavior and its connection with rotational damping have been addressed in cranking model and PRM with single- j shell [29, 30, 31]. The purpose of present work is to study the rotational damping by PRM, in which the angular momentum is a good quantum number and the pairing correlation will be included explicitly. The mechanism of rotational damping and E2 transition property from the region of discrete rotational band into the regime of damped rotational motion will be investigated in a multi- j shell PRM.

II. FORMULATION

A nucleus can be visualized as a rotor coupled with a few valence nucleons, which move more or less independently in the deformed potential of core composed by the rest of the nucleons, i.e., the particles-rotor model (PRM). The Hamiltonian of PRM is expressed as the sum of an intrinsic part and a collective part

$$H_{\text{PRM}} = H_{\text{intr}} + H_{\text{coll}}, \quad (1)$$

where H_{intr} describes microscopically the motion of valence particles near Fermi level and H_{coll} is the collective rotation of core. The intrinsic Hamiltonian is taken as

$$H_{\text{intr}} = \sum_{j_1 m_1 j_2 m_2} \langle j_1 m_1 | -8\kappa \sqrt{\pi/5} Y_{20} | j_2 m_2 \rangle a_{j_1 m_1}^\dagger a_{j_2 m_2} - G \sum_{j' m' j m} a_{j' m'}^\dagger a_{j' \bar{m}'}^\dagger a_{j \bar{m}} a_{j m}, \quad (2)$$

where $a_{j m}^\dagger$ and $a_{j m}$ are the one-particle creation and annihilation operators and a residual pairing interaction has been included. In order to describe many-particle many-hole excitations associated with rotational damping, we include some different- j shells in the deformed

mean-field of valence nucleons. The single-particle energy in the deformed mean-field is written as [29, 32, 33]

$$\sum_{j_1 m_1 j_2 m_2} \langle j_1 m_1 | -8\kappa \sqrt{\pi/5} Y_{20} | j_2 m_2 \rangle a_{j_1 m_1}^\dagger a_{j_2 m_2} = \sum_j \left\{ R_j + \sum_m \kappa \frac{3m^2 - j(j+1)}{j(j+1)} a_{jm}^\dagger a_{jm} \right\}, \quad (3)$$

where R_j is a parameter to indicate the relative energy between different- j shells. The deformation parameter κ is related to the quadrupole deformation β through [31, 34]

$$\kappa \simeq 0.16\hbar\omega_0(N + 3/2)\beta, \quad (4)$$

where $\hbar\omega_0$ is harmonic oscillator frequency of the deformed potential and N the quantum number of the major shell. For example, in the case of $i_{13/2}$ shell, $k = 2.5$ MeV approximately corresponds to $\beta \sim 0.3$, and $h_{9/2}$ shell corresponds to $k = 2.2$ MeV. The two-body correlation between valence particles is taken as pairing interaction with strength parameter G . Since we solve two-body interaction exactly, it will contribute to both particle-particle channel and particle-hole channel.

The spin \vec{I} of nucleus is the sum of angular momentum \vec{R} of core and \vec{J} , the sum of angular momentum of valence nucleons. The collective Hamiltonian can be expressed as

$$H_{\text{coll}} = \frac{R_1^2 + R_2^2}{2\mathcal{J}} = \frac{I^2 - I_3^2}{2\mathcal{J}} + \frac{J^2 - J_3^2}{2\mathcal{J}} - \frac{I_+ J_- + I_- J_+}{2\mathcal{J}}, \quad (5)$$

where $H_{\text{rot}} = (I^2 - I_3^2)/2\mathcal{J}$ describes the nuclear collective rotation. The recoil term $H_{\text{rec}} = (J^2 - J_3^2)/2\mathcal{J}$ acts only on valence nucleons and contains one-body and two-body terms if there is more than one particle outside the core. Coriolis interaction $H_{\text{cor}} = -(I_+ J_- + I_- J_+)/2\mathcal{J}$ couples the collective rotation and the single particle motion.

The eigenfunctions of particles-rotor Hamiltonian can be expanded as

$$\Psi_{IM}^\alpha = \sum_K C_K^\alpha \varphi_{IMK}^\alpha \quad (6)$$

with the mixing coefficient C_K^α , where the symmetrized basis is given by

$$\varphi_{IMK}^\alpha = \sqrt{\frac{2I+1}{16\pi^2(1+\delta_{K0})}} \left\{ \mathcal{D}_{MK}^{I*}(\Omega) \phi_{K\alpha}^{(1,2,\dots,N)} + (-)^{I+K} \mathcal{D}_{M-K}^{I*}(\Omega) \phi_{K\alpha}^{(1,2,\dots,N)} \right\}. \quad (7)$$

$\mathcal{D}_{MK}^I(\Omega)$ is the usual rotation matrix and $\phi_{K\alpha}^{(1,2,\dots,N)}$ the N -body anti-symmetrized wave function of valence particles.

The stretched E2 transition probability from an initial nuclear state α at spin $I + 2$ to a final state α' at I is

$$B(E2, \alpha I + 2 \rightarrow \alpha' I) = \frac{5}{16\pi} Q_0^2 M_{\alpha I + 2, \alpha' I}^2, \quad (8)$$

where the amplitude

$$M_{\alpha I + 2, \alpha' I} = \sum_{KK'} C_K^\alpha(I + 2) C_{K'}^{\alpha'}(I) \langle IK' 20 | I + 2K \rangle \delta_{KK'}. \quad (9)$$

We neglect the minor contribution of non-collective E_2 transition from valence particles since the electric quadrupole moment Q_0 is much larger than that from valence particles. The CG coefficient $\langle IK' 20 | I + 2K \rangle$ represents the coupling of angular momenta in the intrinsic frame. The normalized E2 transition probability $S_{\alpha I + 2, \alpha' I}$ is defined as

$$S_{\alpha I + 2, \alpha' I} \equiv M_{\alpha I + 2, \alpha' I}^2, \quad (10)$$

which satisfies $\sum_{\alpha'} S_{\alpha I + 2, \alpha' I} = 1$ from an initial state α to many final states α' .

III. RESULTS AND DISCUSSIONS

In present PRM, we consider eight valence particles in a multi- j shell coupled with a deformed core. The calculation has been performed with the parameters: the pairing strength $G = 0.45$ MeV, the moment of inertia $\mathcal{J} = 76.0 \text{ } \hbar^2 \text{MeV}^{-1}$, $\kappa = 2.5$ MeV for $i_{13/2}$ intruder orbit and $\kappa = 2.2$ MeV for other shells. These parameters have been used in earlier studies and are considered to be reasonable [19, 29, 31].

In order to imitate the level scheme of Nilsson diagram [35], we include the shells $h_{9/2}$, $i_{13/2}$, $p_{3/2}$, $f_{5/2}$ and $p_{1/2}$ in the deformed mean-field. The relative energies R_j between different- j shells are determined according to spherical Nilsson level diagram. Table I gives the relative energy R_j between shell $h_{9/2}$ and other shells $i_{13/2}$, $p_{3/2}$, $f_{5/2}$ and $p_{1/2}$, e.g. it has been taken as $0.1 \hbar\omega_0$ between shells $h_{9/2}$ and $i_{13/2}$. The choice of these parameters for the present single-particle levels is similar as the neutron levels in nucleus ^{168}Yb . Of course, the valence proton excitations should be included as well to fully understand nucleus ^{168}Yb . However, if both proton and neutron excitations are taken into account, the Hamiltonian matrix will be too big to be diagonalized exactly. In Refs. [27, 28], only one proton and one neutron are coupled with the rotor, and the many-particle and many-hole excitations are thus missing.

The level scheme thus obtained is shown in Fig. 1, in which the spherical shells and their splitting due to deformation are presented. On the right the third component m_j of angular momentum is given.

After defining the single-particle basis, the many-particle many-hole excitations within a given excitation energy form the shell model basis states. The configuration space is spanned by various excitations of eight valence particles in the deformed mean-field. The off-diagonal Hamiltonian from pairing correlation, recoil term and coriolis interaction will mix states not only in the same- j shell, but also in different- j shells [36, 37]. They are responsible for the many-particle many-hole excitations. In the model diagonalization for each spin $I = 0 - 60 \hbar$, the configuration truncation is done with the excitation energy $\sim 0.6 \hbar\omega_0$, which corresponds to the lowest 2000 many-particle many-hole configurations. Most of these configurations has $1p - 1h$ to $4p - 4h$ characters and few of them is with $5p - 5h$ to $6p - 6h$ characters.

Fig. 2 displays the calculated nuclear states with small horizontal bars. Strong E2 transitions satisfying condition $S_{\alpha I+2, \alpha' I} > 1/\sqrt{2} = 0.707$ are plotted with solid lines. Weaker transitions defined by condition $0.5 < S_{\alpha I+2, \alpha' I} < 0.707$ are presented with dashed lines. One may observe that most of the strong E2 transitions lies in the region near yrast line, where the rotational band structure is identified. At higher excitation energy the transitions become much weaker and E2 transition from an initial state may spread out over many final states, implying the disappearance of rotational band structure.

In order to understand the nature of nuclear state, a quantity, occupation number of single-particle basis $[l j m_j]$ in nuclear state α , is defined as

$$P_{l j m_j} = \sum_{\alpha(l j m_j)} C_K^{\alpha 2}, \quad (11)$$

satisfying condition that the sum of various occupancy on single-particle basis is equal to the number of valence particles

$$\sum_{l j m_j} P_{l j m_j} = N. \quad (12)$$

Here we use quantum numbers $[l j m_j]$ to denote the single particle basis states in Fig. 1. Fig. 3 gives the occupation number of particle for various single-particle basis $[l j m_j]$ as a function of angular momentum for (a) ground state band; (b) a strong transition band at excitation energy $U \sim 0.8$ MeV; (c) a weak transition band at excitation energy $U \sim 1.6$

MeV. The lines with filled upper triangle, cross, filled circle, open square, open circle, filled squire and open upper triangle represent the single-particle basis states $[5\frac{9}{2}\frac{1}{2}]$, $[6\frac{13}{2}\frac{1}{2}]$, $[5\frac{9}{2}\frac{3}{2}]$, $[6\frac{13}{2}\frac{3}{2}]$, $[6\frac{13}{2}\frac{5}{2}]$, $[5\frac{9}{2}\frac{5}{2}]$ and $[6\frac{13}{2}\frac{7}{2}]$ separately. Since the occupancy on other higher single particle basis is not important for the low excited states, we use the lines with star to represent the occupancy on those single particle basis. One may observe for the bands satisfying strong transition condition as shown in Fig. 3 (a) and (b), the occupation number of particle is nearly independent of angular momentum. With the increase of excitation energy, the dependence of occupancy on spin becomes more sensitive, as shown for the band with weak transition in Fig. 3 (c). Since the occupancy characterizes the wave function property of nuclear state, these figures clearly indicate how the rotational band structure starts to disappear gradually due to the change of wave function in nuclear states.

In the experiments, strong E2 transitions are observed as discrete peaks in the gamma-ray spectra and the rest of transitions shows up as quasi-continuum spectra which contain transitions summed over many final states. For such a situation, it is useful to represent the E2 transition property by means of strength distribution function. The strength function for a state α at spin $I + 2$ is given by [19]

$$S_{\alpha,I+2}(E_\gamma) = \sum_{\alpha'} S_{\alpha I+2, \alpha' I} \delta(E_\gamma - E_{\alpha I+2} + E_{\alpha' I}). \quad (13)$$

The fragmentation of E2 strength function is the rotational damping phenomenon. In order to quantify the onset of rotational damping, the branch number is defined as

$$n_{\text{branch}}(\alpha I + 2) \equiv \left(\sum_{\alpha'} S_{\alpha I+2, \alpha' I}^2 \right)^{-1}. \quad (14)$$

It counts effectively the branch number of E2 transitions from an initial state α at $I + 2$ to the final states α' , which are allowed by the selection rules of the gamma-ray radiation. For a case where a given state decays to only one final state at the lower spin, n_{branch} is equal to one. If there are two possible transitions with equal probability, the branch number is equal to two. In other words, $n_{\text{branch}} < 2$ implies that the transition from a given state mainly decays to one final state, where the discrete rotational band structure is identified. In contrast, $n_{\text{branch}} > 2$ states that the transitions spread over two or more final states, where the rotational damping takes place.

In order to indicate the E2 transition property more precisely, the strength function $S_{\alpha,I}(E_\gamma)$ is shown in Fig. 4 for the lowest 9 states with $I^\pi = 30^+$. The branch number

n_{branch} and excitation energy U are put for each state. The E2 transition associated with the first 30^+ state exhausts most of the total strength at gamma-ray energy 0.92 MeV. The 30_2^+ , 30_3^+ , 30_4^+ and 30_5^+ states show essentially the same E2 distributions except for slight difference in the gamma-ray energy. The E2 decays from the 30_6^+ , 30_7^+ , 30_8^+ and 30_9^+ states display a different E2 strength distribution, being fragmented over several transitions, each of which carries a rather weak strength. Fig. 5 displays the quantity $S_{\alpha,I}(E_\gamma)$ associated with the states 30_{35}^+ and 30_{36}^+ lying at excitation energy $U \sim 2.3$ MeV, and the states 30_{97}^+ and 30_{98}^+ lying at $U \sim 3.1$ MeV. The E2 strength distribution at $U \sim 2.3$ MeV has about 16 branches, while the number of branches becomes around 42 at $U \sim 3.1$ MeV. It indicates that the degree of the mixing between many-particle many-hole configurations becomes stronger as excitation energy increases, which is the basic mechanism to form the damping of collective rotational motion.

As the excitation energy increases, the rotational band structure gradually disappears and rotational damping takes place. Branching number is a key quantity to measure where rotational damping takes place and the degree of configuration mixing. The dependence of branching number on excitation energy is shown in Fig. 6 for spins (a) $I^\pi = 20^+$, (b) $I^\pi = 30^+$ and (c) $I^\pi = 40^+$. The histogram gives the average branch number within the energy bins. One may observe that branching number increases with excitation energy. Using the criterion $n_{\text{branch}} = 2$ for the onset of rotational damping, the onset energy is predicted to be around excitation energy $U \sim 1.1$ MeV above yrast line.

It should be noted, although the onset energy defined by condition $n_{\text{branch}} = 2$ tells approximately where the rotational damping takes place, the transition from the region of rotational bands to rotational damping is not very sharply at the onset energy, but develops gradually as the excitation energy increases. As shown in Fig. 2, there exist some rotational bands in the region of rotational damping, where the excitation energy is higher than the onset energy. These band structures are surrounded by states which do not have strong transitions. It indicates that the rotational band structure partly remains even in the region of rotational damping. Such feature of rotational bands is also displayed in Fig. 6, where there exist states whose branching number is smaller than 2 at higher excitation energy.

Due to the onset of rotational damping, the number of rotational bands existing in a given nucleus is thus limited and gives a quantitative measure of rotational damping. Here, the number of rotational bands corresponds to the experimental effective number of paths

which can be obtained from $E_\gamma \times E_\gamma$ spectrum by the fluctuation analysis method [8, 9]. Theoretically the number of rotational bands is defined by the number of states with strong E2 transition, which satisfies condition $S_{\alpha I+2, \alpha' I} > 0.707$ or $n_{\text{branch}} < 2$ with at least two consecutive steps $I + 2 \rightarrow I \rightarrow I - 2$ of E2 decays [19]. Since the configuration of valence nucleons occupancy in present model corresponds to rare-earth nucleus ^{168}Yb considered as a core ^{160}Yb plus eight valence neutrons and in our calculation the moment of inertia is taken as the value of rare-earth nucleus, we will make a qualitative comparison between our calculated number of rotational bands and the experimental data for nucleus ^{168}Yb , though the model space in present calculation is not really realistic for nucleus ^{168}Yb . For this nucleus there exists experimental data from the analysis of quasi-continuum gamma-spectra as well as data from discrete spectra identifying the rotational bands up to spin $I \sim 40$ [38, 39]. Fig. 7 shows the calculated number of rotational bands as well as the experimental effective number of paths [9] for nucleus ^{168}Yb . The solid line represents the result with the criterion $S_{\alpha I+2, \alpha' I} > 0.707$ while the dashed line is calculated with condition $n_{\text{branch}} < 2$. The horizontal axis denotes the average gamma-ray energy $E_\gamma = (E_{\gamma_1} + E_{\gamma_2})/2$, where E_{γ_1} is the transition energy for $I + 2 \rightarrow I$ and E_{γ_2} for transition $I \rightarrow I - 2$. It is clear that the two conditions give essentially the same number of rotational bands around 30, and the theoretical calculation agrees well with the experimental result in all the gamma-ray energy range.

In order to study the effect of pairing correlation between valence nucleons on rotational damping, Fig. 8 displays the calculated number of rotational bands with and without pairing correlation, together with experimental result. The solid line represents the result without pairing interaction between valence nucleons, while the dashed line is with the standard pairing $G = 0.45$ MeV. The criterion $S_{\alpha I+2, \alpha' I} > 0.707$ has been used to obtain the number of rotational bands. It is seen that the calculated number of bands becomes much larger when the pairing is turned off. In other words, the rotational band structure has strengthened and rotational damping has weakened when pairing $G = 0.0$ MeV. This indicates that pairing correlation has a significant effect on the damping of rotational motion.

To understand the nature of nuclear state without pairing correlation, Fig. 9 gives the occupation number of particle of the same bands as in Fig. 3, but with pairing strength $G = 0.0$ MeV. One may observe for these bands the dependence of occupancy on spin becomes weaker in the case of without pairing correlation. Especially in low angular momentum,

there is much difference between the occupancy with and without pairing. These results are consistent with the calculation in Fig. 8, where the number of rotational bands becomes larger when paring $G = 0.0$ MeV. It indicates that pairing correlation has an important effect on the nature of nuclear states especially in low angular momentum.

It should be mentioned that pairing correlation between valence nucleons has contributions to both diagonal and off-diagonal Hamiltonians. Diagonal Hamiltonian characterizing the property of mean-field favors the rotational band structure and retards the rotational damping, whereas the off-diagonal Hamiltonian characterizing the quantum fluctuations coming from residual interaction causes the mixing of many-particle many-hole configurations and prefers the rotational damping. Therefore, the delicate balance between the competition of diagonal and off-diagonal components of pairing correlation has determined the appearance of rotational damping. It is concluded that the off-diagonal components of pairing correlation (two-body residual interaction) play an important role in the appearance of rotational damping.

IV. CONCLUSIONS

The damping of collective rotational motion is discussed in a multi- j shell particles-rotor model, in which the angular momentum is strictly conserved and the pairing correlation is included explicitly. It is found that the rotational damping takes place at about 1.1 MeV above yrast line, and the number of states which form rotational band structure is thus limited. The onset energy in present calculation is similar as the theoretical prediction $U \sim 0.8$ MeV in cranked Nilsson mean-field combined two-body residual interaction. The calculated number of rotational bands around 30 is in a qualitative agreement with experimental result in the gamma-ray energy range. The onset of rotational damping takes place quite gradually as a function of excitation energy. Even in the region of rotational damping, there still remains part of discrete rotational band structure. Our calculation clearly indicates that the pairing correlation has an important effect on the nature of nuclear states, especially in low angular momentum. It is found that the calculated number of bands becomes much larger in the case of pairing strength $G = 0.0$ MeV. The pairing correlation between valence particles has significant effect on the appearance of rotational damping. It is noted that the pairing correlation and the exact treatment on angular momentum coupling in PRM play an impor-

tant role to provide a description on rotational damping. However in the cranked Nilsson mean-field combined two-body residual interaction, the rotational damping is attributed to the high-multipole component of two-body residual interaction [19]. Considering that the angular momentum in Ref. [19] is not treated properly and the valence nucleons states are schematic in present model, more works along these lines are necessary to understand better the mechanism of rotational damping.

Acknowledgments

This work was supported in part by the Japan Society for the Promotion of Science (JSPS) and the China National Natural Science Foundation (CNSF) as the bilateral program between Japan and China. The partial supports from the Major State Basic Research Development Program Under Contract Number G2000077407, the National Natural Science Foundation of China under Grant No. 10025522, 10221003, 10375001, and 10435010, the Doctoral Program Foundation from the Ministry of Education in China, and the Knowledge Innovation Project of the Chinese Academy of Sciences under Grant No. KJCX2-SW-N02 are acknowledged.

- [1] G. A. Leander, Phys. Rev. **C 25** (1982) 2780.
- [2] B. Lauritzen, T. Døssing and R. A. Broglia, Nucl. Phys. **A 457** (1986) 61.
- [3] J. C. Bacelar, G. B. Hagemann, B. Herskind, B. Lauritzen, A. Holm, J. C. Lisle and P. O. Tjøm, Phys. Rev. Lett. **55** (1985) 1858.
- [4] J. E. Draper, E. L. Dines, M. A. Deleplanque, R. M. Diamond and F. S. Stephens, Phys. Rev. Lett. **56** (1986) 309.
- [5] F. S. Stephens, J. E. Draper, J. L. Egido, J. C. Bacelar, E. M. Beck, M. A. Deleplanque and R. M. Diamond, Phys. Rev. Lett. **57** (1986) 2912.
- [6] F. S. Stephens, J. E. Draper, J. C. Bacelar, E. M. Beck, M. A. Deleplanque and R. M. Diamond, Phys. Rev. Lett. **58** (1987) 2186.
- [7] F. S. Stephens, J. E. Draper, M. A. Deleplanque, R. M. Diamond and A. O. Macchiavelli, Phys. Rev. Lett. **60** (1988) 2129.

[8] B. Herskind, A. Bracco, R. A. Broglia, T. Døssing, A. Ikeda, S. Leoni, J. Lisle, M. Matsuo and E. Vigezzi, Phys. Rev. Lett. **68** (1992) 3008.

[9] T. Døssing, B. Herskind, S. Leoni, M. Matsuo, A. Bracco, R. A. Broglia, and E. Vigezzi, Phys. Rep. **268** (1996) 1.

[10] B. Herskind, T. Døssing, S. Leoni, M. Matsuo and E. Vigezzi, Prog. Part. Nucl. Phys **28** (Pergamon, 1992) p.235.

[11] B. Herskind, T. Døssing, D. Jerrestam, K. Schiffer, S. Leoni, J. Lisle, R. Chapman, F. Khazaie and J. N. Mo, Phys. Lett. B **276** (1992) 4.

[12] B. Herskind, T. Døssing, S. Leoni, M. Matsuo N. Nica, D. C. Radford and P. Rasmussen, Nucl. Phys. **A 557** (1993) 191c.

[13] S. Leoni, B. Herskind, T. Døssing, P. Rasmussen, P. Bosetti, A. Bracco, R. Broglia, S. Frattini, M. Matsuo, N. Nica, E. Vigezzi, A. Atac, M. Bergström, A. Brockstedt, H. Carlsson, P. Ekström, F. Ingebretsen, H. J. Jensen, J. Jongman, G. B. Hagemann, R. M. Lieder, T. Lönnroth, A. Maj, B. Million, A. Nordlund, J. Nyberg, M. Piiparinen, H. Ryde, M. Sugawara, P. O. Tjøm and A. Virtanen, Nucl. Phys. **A 587** (1995) 513.

[14] S. Frattini, A. Bracco, S. Leoni, F. Camera, B. Million, N. Blasi, G. Lo Bianco, M. Pignanelli and E. Vigezzi et al., Phys. Rev. Lett. **83** (1999) 5234.

[15] F. S. Stephens, M. A. Delephanque, I. Y. Lee, D. Ward, P. Fallon, M. Cromaz, R. M. Clark, R. M. Diamond, A. O. Macciavelli and K. Vetter, Phys. Rev. Lett. **88** (2002) 142501.

[16] T. Guhr and H. A. Weidenmüller, Ann. Phys. **A 193** (1989) 489.

[17] J. L. Egido and A. Faessler, Z. Phys. **A 339** (1991) 115.

[18] M. Matsuo, T. Døssing, E. Vigezzi, R. A. Broglia, Phys. Rev. Lett. **70** (1993) 2694.

[19] M. Matsuo, T. Døssing, E. Vigezzi, R. A. Broglia and K. Yoshida, Nucl. Phys. **A 617** (1997) 1.

[20] M. Matsuo, T. Døssing, E. Vigezzi, S. Åberg Nucl. Phys. **A 620** (1997) 296.

[21] K. Yoshida, M. Matsuo, Nucl. Phys. **A 612** (1997) 26.

[22] K. Yoshida, M. Matsuo, Nucl. Phys. **A 636** (1998) 169.

[23] M. Matsuo, K. Yoshida, T. Døssing, E. Vigezzi and R. A. Broglia, Nucl. Phys. **A 649** (1999) 379.

[24] T. Døssing, B. Herskind, M. Matsuo, S. Leoni, A. Bracco, E. Vigezzi and R. A. Broglia, Nucl. Phys. **A 682** (2001) 439.

- [25] K. Yoshida, M. Matsuo, Y. R. Shimizu, Nucl. Phys. **A 696** (2001) 85.
- [26] J. Meng, Acta Physics Sinica(in Chinese)**42** (1993) 368.
- [27] S. Frauendorf, and J. Meng, Z. Phys.**A356** (1996) 263.
- [28] S. Frauendorf, and J. Meng, Nucl. Phys. **A617** (1997) 131.
- [29] A. T. Kruppa and K. F. P  , Phys. Rev. **C52** (1995) 1818.
- [30] S.   berg, Phys. Rev. Lett. **64** (1990) 3119.
- [31] J. A. Sheikh and Y. Sun, Nucl. Phys. **A 733** (2004) 67.
- [32] I. Hamamoto, Nucl. Phys. **A 271** (1976) 15.
- [33] R. Bengtsson and H. Hakansson, Nucl. Phys. **A 357** (1981) 61.
- [34] J. A. Sheikh, D. D. Warner, P. Van Isacker, Phys. Lett. **B 433** (1998) 16.
- [35] P. Ring, P. Schuck, The Nuclear Many-Body Problem (Springer-Verlag, 1980).
- [36] L. Guo, X. R. Zhou, J. Meng, E. G. Zhao, Commun. Theor. Phys. 37 (2002) 323.
- [37] X. R. Zhou, L. Guo, J. Meng, E. G. Zhao, Commun. Theor. Phys. 37 (2002) 583.
- [38] A. Fitzpatrick, S. A. Araddad, R. Chapman, J. Copnell, F. Lind'en, J. C. Lisle, A. G. Smith, J. P. Sweeney, D. M. Thompson, W. Urban, S. J. Warburton, J. Simpson, C. W. Beausang, J. F. Sharper-Shafer, S. J. Freeman, S. Leoni and J. Wrzesinski, Nucl. Phys. **A 585** (1995) 335.
- [39] J. R. B. Oliveira, S. Frauendorf, M. A. Deleplanque, R. M. Diamond, F. S. Stephens, C. W. Beausang, J. E. Draper, C. Duyar, E. Rubel, J. A. Becker, E. A. Henry and N. Roy, Phys. Rev. **C47** (1993) R926.

TABLE I: The relative energy R_j between shell $h_{9/2}$ and other shells $i_{13/2}$, $p_{3/2}$, $f_{5/2}$ and $p_{1/2}$ in unit of $\hbar\omega_0$. The level scheme is shown on the left in Fig. 1.

R_j	$i_{13/2}$	$p_{3/2}$	$f_{5/2}$	$p_{1/2}$
$h_{9/2}$	0.1	0.3	0.35	0.49

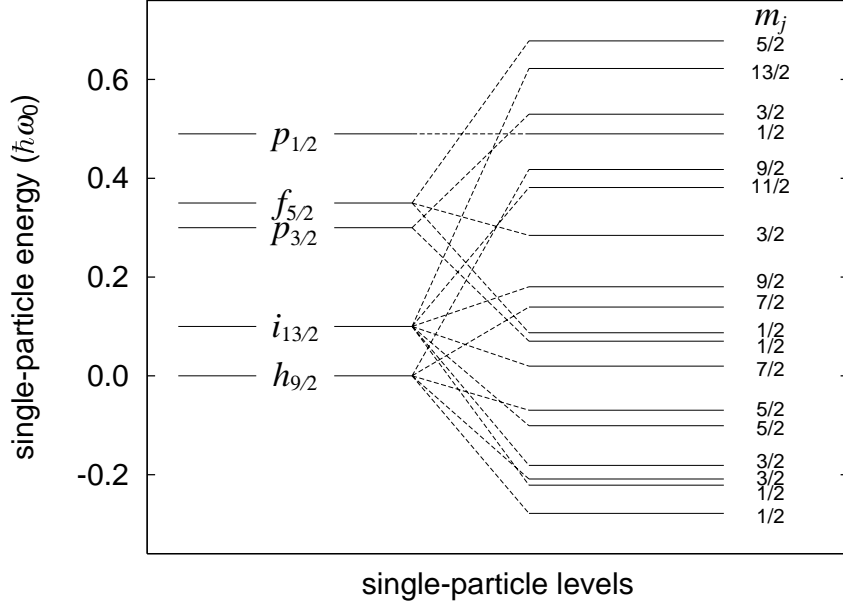


FIG. 1: Single-particle level scheme in the mean-field of valence particles. The spherical shells on the left split up to the structure on the right due to the deformation with the third component m_j of angular momentum.

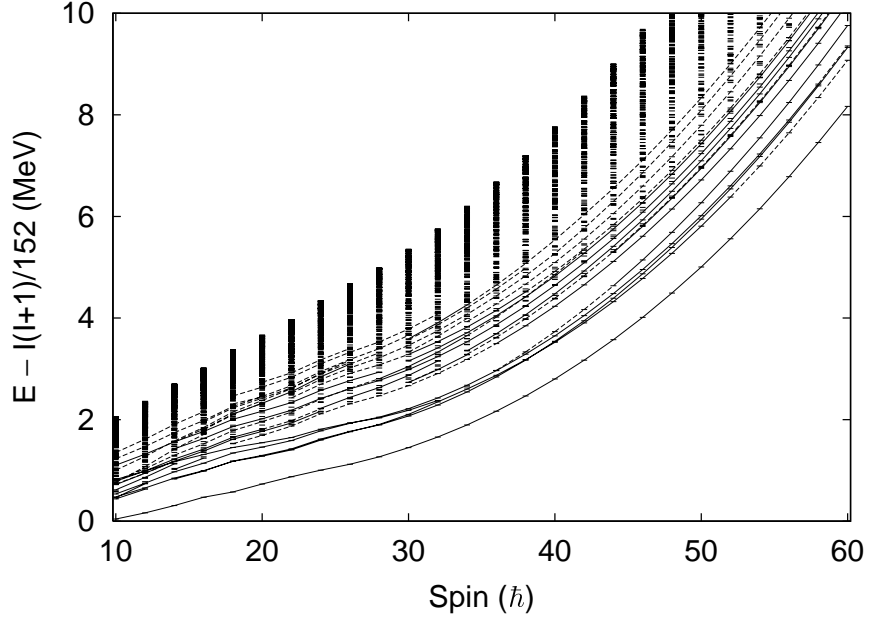


FIG. 2: The calculated nuclear states are plotted with small horizontal bars. A reference energy $I(I+1)/2\mathcal{J}$ with $\mathcal{J}=76.0 \hbar^2 \text{MeV}^{-1}$ is subtracted. Solid lines connecting the energy levels represent the strong E2 transitions which have the normalized strength $S_{\alpha I+2, \alpha' I}$ larger than 0.707. Dashed lines are the weaker E2 transitions with normalized strength between 0.5 and 0.707.

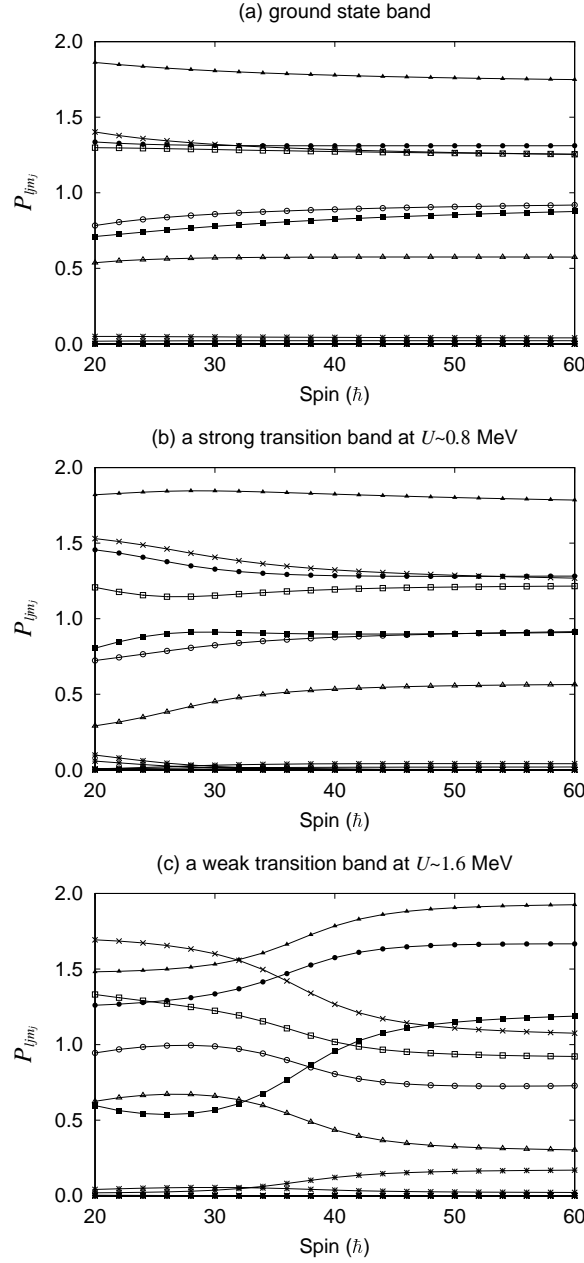


FIG. 3: Occupation number of particle for various single-particle basis $[l j m_j]$ as a function of spin for (a) ground state band; (b) a strong transition band at excitation energy $U \sim 0.8$ MeV; (c) a weak transition band at excitation energy $U \sim 1.6$ MeV. The lines with filled upper triangle, cross, filled circle, open square, open circle, filled squire and open upper triangle represent the single-particle basis states $[5\frac{9}{2}\frac{1}{2}]$, $[6\frac{13}{2}\frac{1}{2}]$, $[5\frac{9}{2}\frac{3}{2}]$, $[6\frac{13}{2}\frac{3}{2}]$, $[6\frac{13}{2}\frac{5}{2}]$, $[5\frac{9}{2}\frac{5}{2}]$ and $[6\frac{13}{2}\frac{7}{2}]$ separately. The lines with star denote the occupancy on other single particle basis.

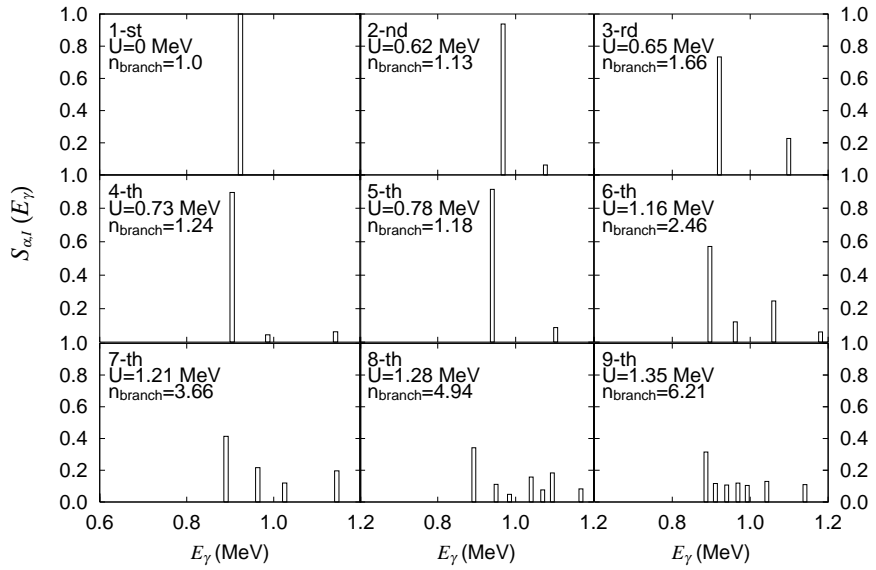


FIG. 4: The E2 strength distribution $S_{\alpha,I}(E_{\gamma})$ from the lowest 9 states with $I^{\pi} = 30^{+}$. The branch number n_{branch} and excitation energy U are put for each state.

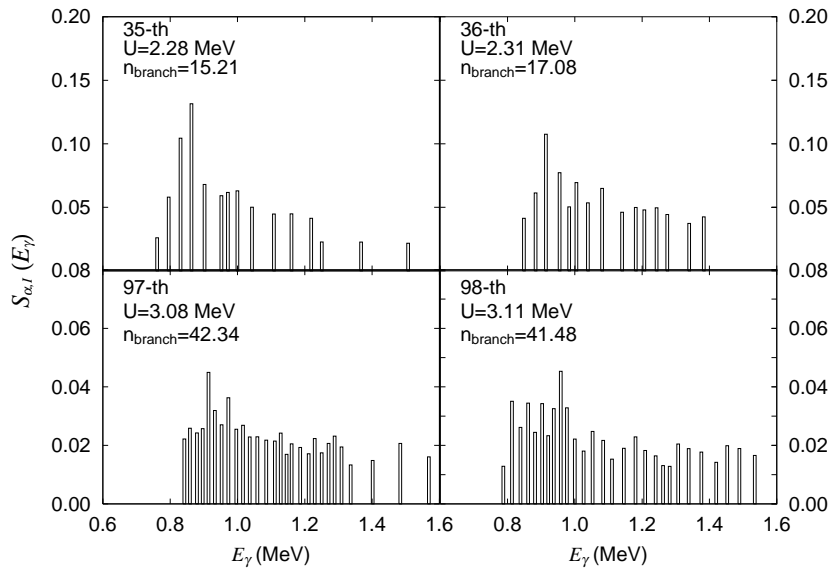


FIG. 5: The strength distribution $S_{\alpha,I}(E_{\gamma})$ for the stretched E2 decays from the 35th and 36th, 97th and 98th excited states with $I^{\pi} = 30^{+}$.

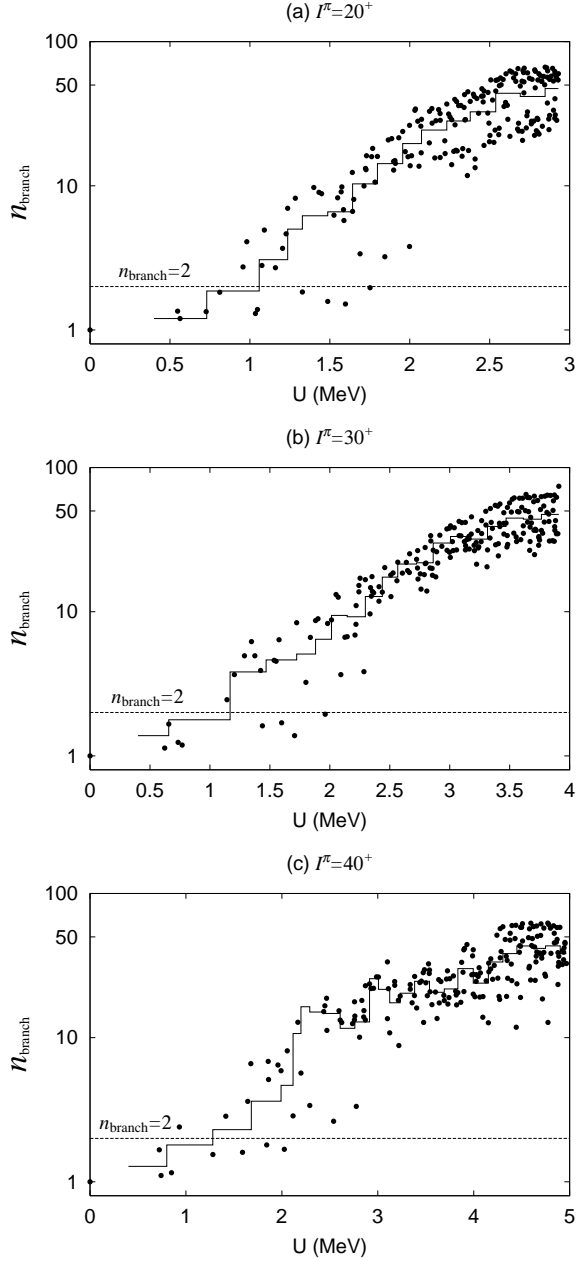


FIG. 6: The branching number n_{branch} for (a) $I^\pi = 20^+$, (b) $I^\pi = 30^+$ and (c) $I^\pi = 40^+$ as a function of excitation energy U . The histogram gives the average branch number within the energy bins. The horizontal line shows $n_{\text{branch}}=2$ used to define the onset of rotational damping.

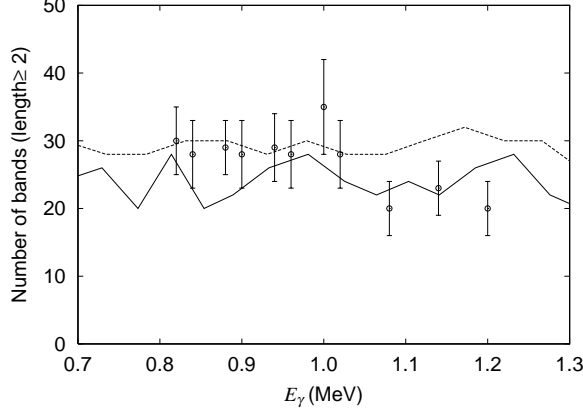


FIG. 7: The calculated number of bands together with the experimental effective number of paths for nucleus ^{168}Yb [9] as a function of the average transition gamma-ray energy. The solid line is calculated with the criterion $S_{\alpha I+2, \alpha' I} > 0.707$ while the dashed line represents the result with condition $n_{\text{branch}} < 2$.

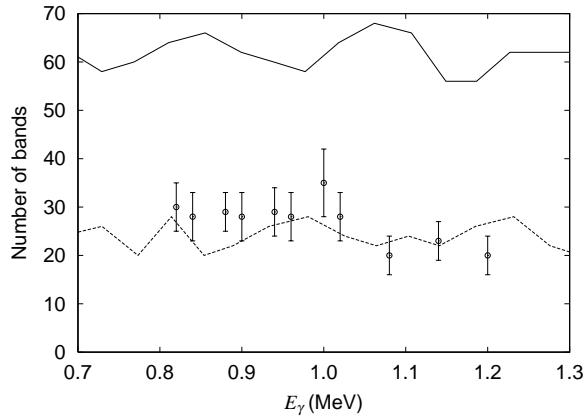


FIG. 8: The calculated number of bands with and without pairing correlation together with the experimental result as a function of the average gamma-ray energy. The solid line is the result with pairing strength $G = 0.0$ MeV, while the dashed line is with the standard pairing $G = 0.45$ MeV. The criterion $S_{\alpha I+2, \alpha' I} > 0.707$ has been used to obtain the number of rotational bands.

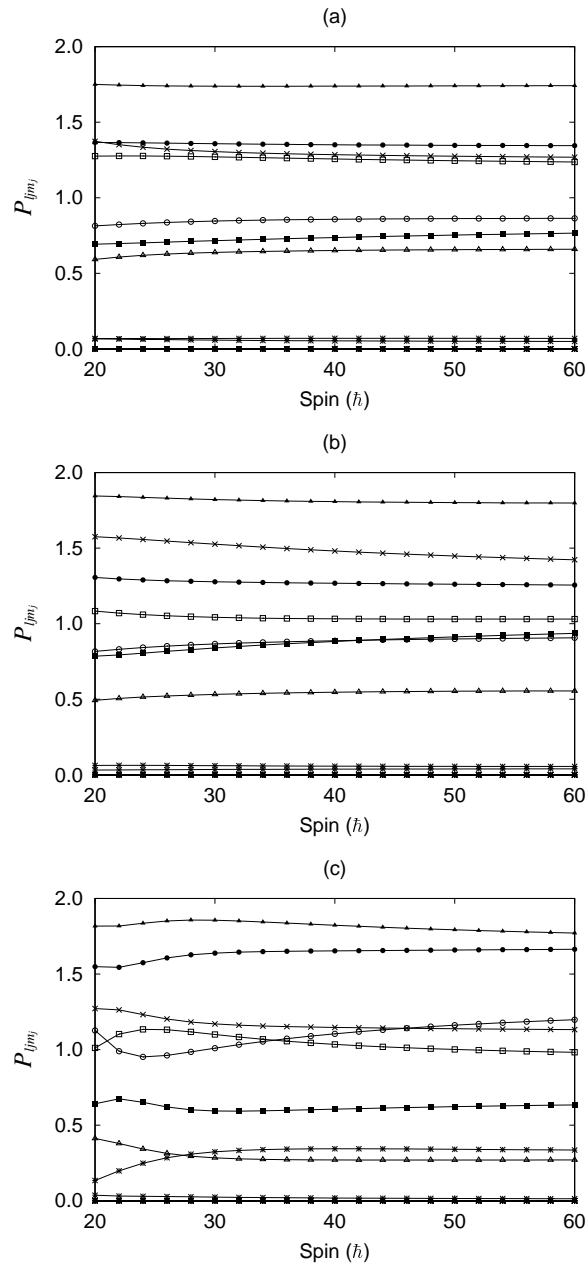


FIG. 9: The same as in Fig. 3, but without pairing correlation.